Model Uncertainties in FEM Analyses of Punching Failures of Concrete Slabs

Model Uncertainties in FEM Analyses of Punching Failures of Concrete Slabs

Model Uncertainties in FEM Analyses of Punching Failures of Concrete Slabs

Gabriele Bertagnoli [1], Benedetto La Fauci [1], Diego Gino [1]

[1] DISEG – Politecnico di Torino, Corso Duca degli Abruzzi, 24 – 10129 Torino, Italy

gabriele-bertagnoli@polito.it

Abstract. Punching shear is a type of failure of reinforced concrete slabs subjected to localized forces. This failure has been examined by many researchers experimentally, analytically or numerically. Empirical equations based on tests observations are nowadays the basis of the existing design codes. The work described herein presents 3D Finite elements method (FEM) analysis of three slab-column connections also tested experimentally to investigate the three fundamental geometries: central, side and corner column. The sensitivity of the FEM response to input parameters such as material constitutive laws is studied. Concrete constitutive models are described in detail, including their effects on the accuracy of FEM analysis. The comparison between FEM results, experimental tests, code provisions and a new model for punching based on the compression chord capacity model is presented. As a conclusion, an estimation of the model uncertainties related to FEM analyses of punching failures without shear reinforcement is discussed.

1. Introduction

Punching shear failure has occurred several times in these past decades [1], [2], [3]; this type of failure is dangerous as it is brittle.

Punching is one of the most critical issues to consider when determining the thickness of flat slabs at the column-slab intersection, so accurate prediction of punching shear strength is a major concern for engineers in order to design a safe structure.

Several researchers have conducted laboratory tests to study the structural behaviour of reinforced concrete slabs supported on columns [4], [5], [6]. The structural response of reinforced concrete slabs supported on interior columns was experimentally investigated by Kinnunen and Nylander (1960) [7]. Their test specimens consisted of circular slab portions supported on circular columns placed in the centre and loaded along the circumference. Based on their test results, these researchers developed a rational theory for the estimation of the punching shear strength in the early 1960s based on the assumption that the punching strength is reached for a given critical rotation ψ. Not only did the model agree well with the test results, it was also the first model that thoroughly described the flow of forces. Kinnunen [6] continued his research on punching shear in 1971 with an investigation on flat slabs supported at their edges. Thus far, this proposal remains one of the best models for the phenomenon of punching. Subsequently, some improvements were proposed by Carl Erik Broms (1990) [8] to account for size effects and the effect of increasing concrete brittleness. While very elegant and leading to good results, Brom's model was never directly included in codes of practice because its application was too complex. Then, Muttoni (2008) [9] gave evidence supporting the role of the shear critical crack in the punching shear strength. Muttoni presented a mechanical explanation of the phenomenon

of punching shear on the basis of the opening of a critical shear crack, providing a formulation of a new failure criterion for punching shear based on the rotation of a slab: the critical shear crack theory. This criterion correctly describes punching shear failures observed in experimental testing. Finally, with an adaption of a previously existing model (compression chord capacity model) for shear strength, authors A. Cladera, et al. [10] incorporate the contribution of the main shear resisting mechanisms. For this purpose, the differences between the shear and punching resistant mechanisms were identified and accounted in order to develop the failure criterion. In this work this last model is not analysed in detail; however, it is validated by comparing laboratory tests on slabs without punching reinforcement with the finite element analysis.

2. Case studies

Three slab-column specimens (*SB1*, *R1* and *No.2*) without shear reinforcement were analysed using the program Midas FEA. The first specimen is the test done by Adetifa and Polak on a column placed in the centre of a slab in 2005 [4], called *SB1.* The second specimen is the corner supported slab called R1 from the experiments conducted by Ingvarsson in 1977 [5]. The third one is the edge supported slab called No.2 by Kinnunen in 1971 [6].

2.1. Case 1: specimen SB1

A concrete slab with square shape 1800x1800mm and 120mm depth is connected to a central column of 150x150mm. This specimen is loaded until failure in displacement control through the column and supported along the edges with restraints applied at 1500x1500 mm distance from the column. The corners of the slabs are held down to simulate continuous slab construction and avoid the slab edges lifting during the test. Details and dimensions are shown in figure 1. For the tension mat, 10M bars at 100 and 90 mm centres are used for the bottom and top layers, respectively. Concrete compressive cylindrical strength, f_c, is 44 MPa, and steel yield strength is 455 MPa.

2.2. Case 2: specimen No.2

A rectangular slab 3000x1800mm and 130mm depth is supported in the middle of its opposite short edges by square concrete columns (see figure 2) and it is unsupported along its longer edges. Also in this case double symmetry was considered, and only ¼ of slab has been modelled. Eight concentrated loads were placed on the slab with regular spacing to simulate uniformly distributed load. Concrete cylindrical compressive strength, f_c, is 26 MPa, and steel yield strength is 420 MPa.

2.3. Case 3: specimen R1

A rectangular slab 1855x2145mm and 120 mm depth is supported on its 4 corners by rectangular concrete columns 145x215mm (see figure 3). This specimen was loaded, with a distributed load applied on the slab, simulated by 16 concentrated loads on a regular path. Concrete compressive strength, f_c, is 28 MPa, and steel yield strength is 470 MPa. Only ¼ of this specimen has been modelled in the FEM analyses because of double axis symmetry.

3. Finite element parametric analyses

The aim of the present paper is to study the sensitivity of finite element analyses simulating punching failures to some model parameters like the concrete constitutive law, the level of ductility available both after tensile cracking (tension softening) and after peak compression (compression softening), and the effect of confinement and lateral cracking on compression law. Three experimental tests representing the three most common configurations for column-slab connection (central, edge and corner column) have been modelled with 15 analyses each. Results are compared with experimental ones and with most diffused code provisions.

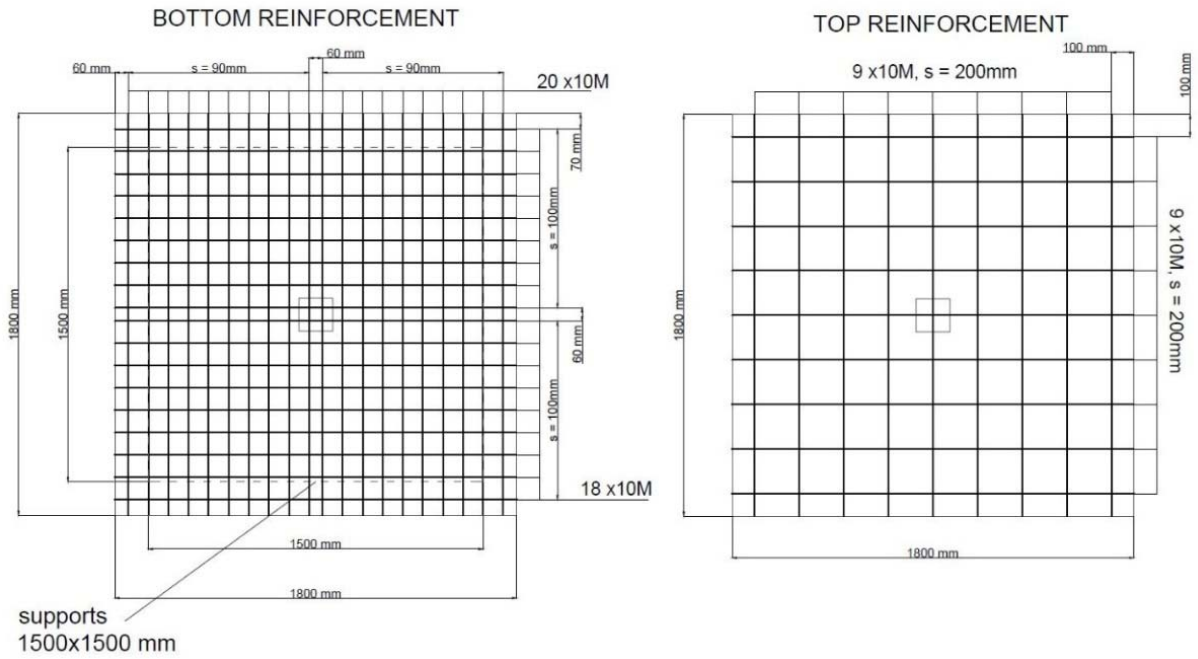

Figure 1. Specimen *SB1*, dimensions and reinforcements

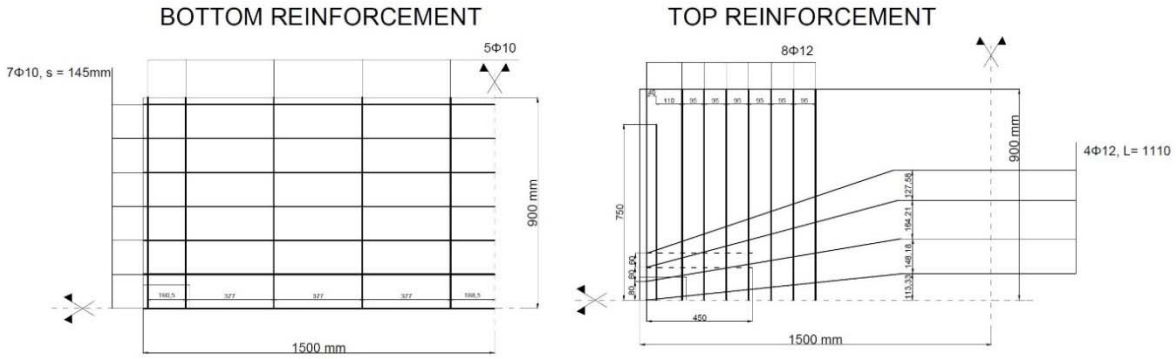

Figure 2. Specimen *No.2*, dimensions and reinforcements

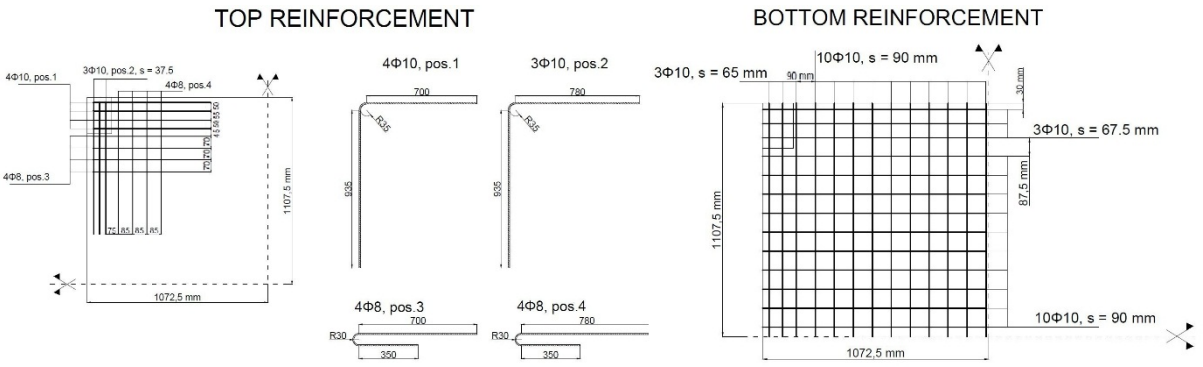

Figure 3. Specimen *R1*, dimensions and reinforcements

4. Material models for concrete

Nonlinear finite element analyses of reinforced concrete structures require proper and adequate definitions of material models. In this work, the "total strain crack model" is used for concrete with the hypothesis of smeared cracking and fixed crack direction. Three constitutive laws are used for concrete compression and one for tension. In addition, the effect of lateral confinement [11] and cracking is taken into account to modify compressive strength and ductility, increasing them with increasing isotropic stress [12] or decreasing them because of lateral cracking [13].

4.1. Constitutive laws for concrete compression

The first constitutive law for concrete compression behaviour is the Thorenfeldt one [12], as given by equation 1.

$$f = -f_p \frac{\varepsilon_i}{\varepsilon_p} \frac{n}{n-1+\left(\frac{\varepsilon_i}{\varepsilon_p}\right)^{nk}} \tag{1}$$

The second constitutive law for concrete compression behaviour is the parabolic model suggested by Feenstra [14], and given by equation 2. It is characterized by three parameters: compressive strength f_c, compressive fracture energy G_c, and crack bandwidth h.

$$\sigma(\varepsilon) = \begin{cases} -f_c \dfrac{1}{3}\dfrac{\varepsilon}{\varepsilon_{p/3}} & if\ \ 0 \le \varepsilon < \varepsilon_{p/3} \\ -f_c \dfrac{1}{3}\left(1+4\left(\dfrac{\varepsilon-\varepsilon_{p/3}}{\varepsilon_p-\varepsilon_{p/3}}\right)-2\left(\dfrac{\varepsilon-\varepsilon_{p/3}}{\varepsilon_p-\varepsilon_{p/3}}\right)^2\right) & if\ \ \varepsilon_{p/3} \le \varepsilon < \varepsilon_p \\ -f_c\left(1-\left(\dfrac{\varepsilon-\varepsilon_p}{\varepsilon_u-\varepsilon_p}\right)^2\right) & if\ \ \varepsilon_p \le \varepsilon < \varepsilon_u \\ 0 & if\ \ \varepsilon_u \le \varepsilon \end{cases} \tag{2}$$

The third constitutive law for concrete compressive behaviour used in this work is the parabolic-rectangle as described in Eurocode 2 [15]. This model depends only on the compressive strength f_c, the peak strain $\varepsilon_{c2} = 2‰$, and the ultimate strain $\varepsilon_{cu} = 3.5‰$.

$$\sigma(\varepsilon) = \begin{cases} 2\dfrac{f_c}{\varepsilon_{c2}}\varepsilon\left(1-\dfrac{\varepsilon}{2\varepsilon_{c2}}\right) & if\ \ \varepsilon \le \varepsilon_{c2} \\ f_c & if\ \ \varepsilon_{c2} \le \varepsilon \le \varepsilon_{cu} \end{cases} \tag{3}$$

4.2. Constitutive law for concrete tension

Hordijk, Cornelissen and Reinhardt [16] proposed an expression for the tension softening behaviour of concrete defined by equation (4).

$$\frac{\sigma^{cr}(\varepsilon')}{f_t} = \begin{cases} \left(1+\left(c_1\dfrac{\varepsilon'}{\varepsilon_{ult}}\right)^3\right)\exp\left(-c_2\dfrac{\varepsilon'}{\varepsilon_{ult}}\right)-\dfrac{\varepsilon'}{\varepsilon_{ult}}(1+c_1^3)\exp(-c_2) & if\ \ 0 < \varepsilon' < \varepsilon_{ult} \\ 0 & if\ \ \varepsilon_{ult} < \varepsilon' \end{cases} \tag{4}$$

where $\varepsilon' = \varepsilon - \varepsilon_{cr}$ is the strain in cracked field, $c_1=3$, $c_2=6.93$ and the ultimate strain is $\varepsilon_{ult} = G_f/(h \cdot f_t)$, where G_f is the tensile fracture energy, f_t is the mean tensile strength, and h is the crack bandwidth as seen in the previous paragraphs.

4.3. Constitutive law for concrete in shear

Shear stiffness can be reduced after cracking in fixed crack models. A constant shear stiffness reduction is chosen: $G_{cr} = \beta \cdot G$, with $\beta=1$ after cracking.

4.4. Calculation of the crack bandwidth h

The influence of the parameter h on the analysis has been studied as it is used in both Feenstra and Hordijk models. For 3D elements the crack bandwidth is suggested to be set equal to the cubic root of the element's volume [17]. The mesh was formed by tetrahedral elements, so initially h has been calculated as $h = \sqrt{V} = 15mm$. Then, using code provisions from EN 1992-1-1[13], all the models were studied using $h = S_{r,max}$ and $h = S_{r,max}/2$ where $S_{r,max}$ is the maximum crack spacing, given by equation (5).

$$S_{r,\max} = k_3 \cdot c + k_1 \cdot k_2 \cdot k_4 \cdot \frac{\phi}{\rho_{p,eff}} \tag{5}$$

4.5. Reinforcement model

Embedded reinforcement approach has been used: the stiffness of the reinforcements is added to the stiffness of the continuum elements in which the reinforcements are located. Steel for reinforcement is modelled according to Von Mises law with perfect plasticity option.

5. Finite elements analysis

The three concrete slabs were modelled with Midas FEA. The mesh of all models was formed by solid tetrahedral elements. Meshed models can be seen in figure 4: specimen *SB1, R1* and *No.2* count respectively 73468, 309502 and 350621 finite elements. Boundary conditions were created considering double axis symmetry for *No.2* and *R1*.

Reported concrete and steel strengths, for the compared specimens, are presented in table 1. The measured value for comparison between numerical and experimental results is the vertical displacement of the column for *SB1* and of the centre of the slabs in models *No.2* and *R1*. The chosen mesh was evaluated to be fairly accurate, as the response from the FE-analyses showed very good agreement with the reported observations. Newton-Raphson iteration method was used, but even if it needed only a few iterations at each load step, it resulted to be relatively time-consuming because of the dimension of the mesh.

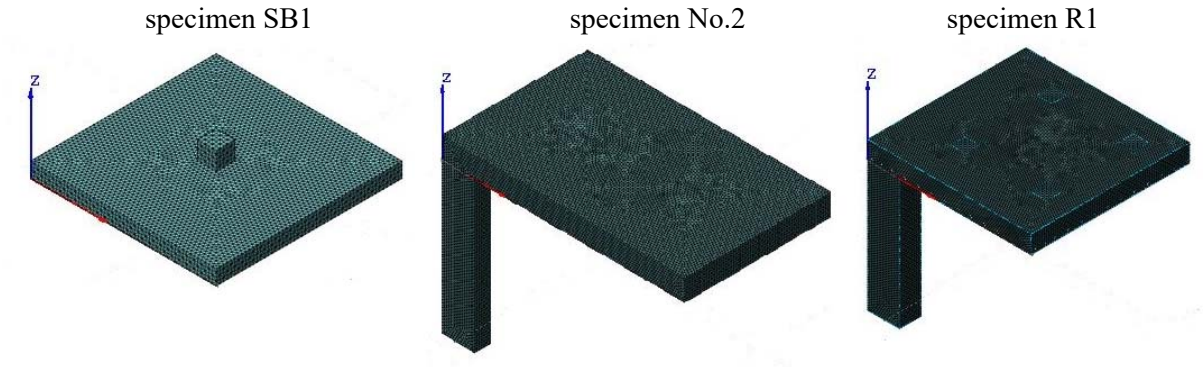

Figure 4. Mesh configurations of specimens

Table 1. Material data used in FEM analysis for each specimen

	f_c [MPa]	f_t [MPa]	υ [-]	G_c [N/mm]	G_f [N/mm]	E_c [MPa]	f_y [MPa]	f_u [MPa]	ε_{sy} [-]	ε_{su} [-]
SB1	44	2.2	0.15	7.00	7.00E-2	28000	455	650	2.28E-3	5%
R1	28	2	0.15	7.25	7.25E-2	29030	470	470	2.35E-3	5%
No.2	26	1.86	0.15	6.91	6.91E-2	28432	420	420	2.10E-3	5%

6. Results and discussions

Each structure has been modelled three times with each compression law (Thorenfeldt, Feenstra and parabolic-rectangle). Three values of crack bandwidth were used for each compression law as described in 4.4 for a total of nine analyses for specimen. The models with Feenstra and Thorenfeldt laws were then run again including confinement and lateral cracking effect (that were not available in the FEM for the parabolic-rectangle law), generating six new outputs for specimen. A total of 15 analyses for specimen was therefore performed.

Numerical results are classified with a code like XX-hYYY-ZZZ where: XX can be Th or Fe or PR respectively for Thorenfeldt, Feenstra or parabolic-rectangle compression curves, h is the crack bandwidth, YYY is its value calculated according 4.4, ZZZ can be NCC for analyses where the effect of lateral compression and lateral cracking is not taken into account or YCC when these two effects are taken into account. The comparison between numerical outputs and experimental ones in term of ultimate load, P_u, and displacement of the reference point, δ_u, is presented in table 2.

Table 2. Results comparison

Specimen		*SB1*		*R1*		*No.2*	
Test No.	Description	*Pu* [kN]	δ_u [mm]	*Pu* [kN]	δ_u [mm]	*Pu* [kN]	δ_u [mm]
	Experimental	**253**	**11.90**	**106.8**	**20.95**	**123.3**	**20.11**
1	Th-h=√V-NCC	258.7	15.16	120.6	23.37	143.3	18.44
2	Th-h=$S_{r,max}$/2-NCC	253.5	15.56	120.6	28.39	148.4	20.36
3	Th-h=$S_{r,max}$-NCC	269.1	15.85	133.1	30.00	153.6	21.10
4	Fe-h=√V -NCC	258.7	13.27	120.6	19.05	138.2	19.52
5	Fe-h=$S_{r,max}$/2-NCC	253.5	15.48	120.6	20.13	148.4	20.17
6	Fe-h=$S_{r,max}$ -NCC	269.1	16.74	124.8	21.12	153.6	22.12
7	Th-h=√V -YCC	258.7	14.28	116.4	17.89	138.2	16.82
8	Th-h= $S_{r,max}$/2-YCC	144.9	5.71	120.6	19.77	158.7	21.36
9	Th-h=$S_{r,max}$ -YCC	181.1	8.79	124.8	20.41	133.1	21.83
10	Fe-h=√V -YCC	258.7	13.27	124.8	20.22	140.8	15.99
11	Fe-h= $S_{r,max}$/2-YCC	248.4	15.41	108.1	20.34	158.7	22.61
12	Fe-h=$S_{r,max}$ -YCC	263.9	17.12	108.1	22.00	168.9	25.02
13	PR-h=√V -NCC	258.7	12.34	116.4	20.87	133.1	19.06
14	PR-h= $S_{r,max}$/2-NCC	269.1	13.92	120.6	22.76	148.4	22.44
15	PR-h=$S_{r,max}$ -NCC	263.9	14.57	120.6	23.29	148.4	23.45

A more detailed comparison is presented for each specimen in the following paragraphs. Some general considerations common to all results follow hereafter. The effect of the bandwidth is common to all models: small values of *h* lead to higher tension stiffening behaviour after cracking: a significant difference is seen between *h*=√V and *h*= $S_{r,max}$/2, whereas small difference is seen between *h*=$S_{r,max}$/2 and h= $S_{r,max}$.

The model that provides the best accuracy in predicting both the ultimate load and displacement of all the specimens is the parabolic-rectangle.

6.1. SB1 results

All models provide good solutions in term of load-displacement curves. The effect of confinement and lateral cracking seems not to affect Feenstra model, whereas it leads to premature failure with Thorenfeldt one in association with higher bandwidths. The model that provides the best accuracy is the parabolic-rectangle in combination with a crack bandwidth equal to h=$\sqrt{V}$=15mm ($P_{u,fem}$ / $P_{u,exp}$ =1.022, $\delta_{u,fem}$ / $\delta_{u,exp}$ = 1.036). Nevertheless, it overestimates the stiffness after first cracking, whereas the same model with h = $S_{r,max}$/2 = 123mm underestimates it. A more correct approximation may be reached with a crack bandwidth 15<*h*<123mm.

6.2. No.2 results

All models provide good solutions in term of ultimate load, but relevant differences can be seen in term of ultimate displacements. The effect of confinement and lateral cracking seems to affect neither Feenstra nor Thorenfeldt model. The model that provides the best accuracy ($P_{u,fem}$ / $P_{u,exp}$ =1.079, $\delta_{u,fem}$ / $\delta_{u,exp}$ =0.947) is the parabolic-rectangle in combination with a crack bandwidth equal to h=15mm that is the cubic root of the element's volume. Nevertheless, it underestimates the stiffness after first cracking, and overestimates it before failure. A more correct approximation may be reached with a crack bandwidth $S_{r,max}$ /2 <*h*< $S_{r,max}$.

6.3. R1 results

All models provide good solutions in term of ultimate load but tend to underestimate the ultimate displacement. The effect of confinement and lateral cracking seems to have nil effect on Feenstra model and very little on Thorenfeldt one. The model that provides the best accuracy ($P_{u,fem}$ / $P_{u,exp}$ =1.089, $\delta_{u,fem}$ / $\delta_{u,exp}$ =0.996) is the parabolic-rectangle in combination with a crack bandwidth equal to h=15mm that is the cubic root of the element's volume. Nevertheless, it underestimates the stiffness after first cracking, and the ultimate displacement.

7. Comparison between experimental results and the one obtained with design codes, CCCM and FEA

The results from the FEA presented in the previous paragraphs are compared to current code provisions (EC2 2004 [18]; ACI 318-2008 [19]; Model Code 2010 [20]) and finally with the Compression Chord Capacity Model (CCCM) proposed by Caldera et al. [10]. Figure 5 shows the ratio of the punching strength predicted by code provisions, FEA and Caldera to the one measured during laboratory tests.

The mean punching shear resistance may be calculated modifying the EC2 provision (6.47) for the design one as follows:

$$v_{R,c} = C_{R,c} \cdot k \cdot \left(100\rho_l \cdot f_{cm}\right)^{1/3} + k_1 \cdot \sigma_{cp} \geq v_{\min} + k_1 \cdot \sigma_{cp} \tag{6}$$

$$V_{R,c} = v_{R,c} \cdot d \cdot u \tag{7}$$

The mean punching shear resistance may be calculated modifying the MC2010 provision (7.3-61) for the design one as follows:

$$V_{Rd,c} = k_\psi \frac{\sqrt{f_{cm}}}{\gamma_c} b_0 d \tag{8}$$

where the parameter k_ψ depends on the deformability of the slab to column joint expressed by means of the rotation ψ as follows:

$$k_{\psi} = 1/\left(1.5 + 0.9k_{dg} \cdot \psi \cdot d\right) \leq 0.6 \tag{9}$$

And the rotation ψ has been calculated according to level one of approximation with the expression:

$$\psi = 1.5\frac{r_s}{d}\frac{f_y}{E_s} \tag{10}$$

The mean punching shear resistance according to ACI 318-2008 may be calculated as the smallest of the following three values (in US customary units):

$$V_c = \min\left\{\left(2+\frac{4}{\beta}\right)\lambda\sqrt{f_{cm}}b_{1,red}d\,;\left(\frac{\alpha_s d}{b_0}+2\right)\lambda\sqrt{f_{cm}}b_{1,red}d\,;4\lambda\sqrt{f_{cm}}b_{1,red}d\right\} \tag{11}$$

The mean punching shear resistance according to CCCM [10] can be written as:

$$\min\begin{cases}V_y \\ V_{cu} \geq v_{c,\min}\end{cases} \tag{12}$$

where V_y is the strength corresponding to steel yielding and V_{cu} is the strength on concrete side. Their values are given by:

$$V_y = 2\pi\,\rho_l f_{ym} d^2\left(1-\frac{\rho f_{ym}}{2f_{cm}}\right) \tag{13}$$

$$V_{cu} = \xi\left(1.125\frac{x}{d}+0.425\right)f_{ctm}b_{1,red}d \tag{14}$$

The numeric values of the key parameters involved in code equations are presented in table 3.
In figure 5 the results of the FEA are plotted as coloured points and the prediction obtained using the four theoretical models cited above are shown with coloured lines. The ratio between the predicted failure load and the experimental one is plotted for each solution.

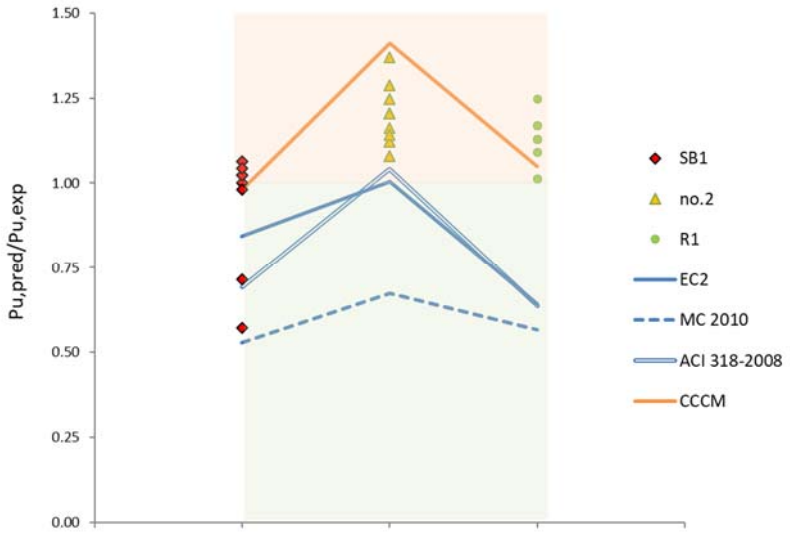

Figure 5. Ratio of the predicted (numerical or analytical) punching strength to experimental one

The three codes and the CCCM theory present the same behaviour, showing for specimen No.2 a higher ratio $P_{u,pred}/P_{u,exp}$ than for the other two specimens. CCCM theory shows a better overall behaviour, but it strongly overestimates the failure load of specimen No.2. EC2 model is always on the safe side, but it underestimates the failure load of specimen R1. ACI shows almost the same response of EC2, but it gives a lower prediction of the failure load of specimen SB1. MC 2010 with Level 1 approach heavily underestimates all the tests, and therefore provides the worst performance. This result may be due to the approximation related to LV1, but it is nevertheless an important remark. Last, but not least, the dispersion of the results obtained using four different theories is incredibly high.

Table 3. Punching resistance parameters

	f_{cm} [MPa]	d [mm]	ρ_l [%]	u [mm]	$b_{1,red}$ [mm]	b_0 [mm]	r_s [mm]	ψ_{LV1} [rad]
SB1	44	90	1.3	1731	883	794	330	2.84E-2
No.2	28	100	1.1	1228	757	530	616	2.21E-2
R1	26	90	2.0	553	431	280	220	0.98E-2

8. Conclusions

The present paper studies the sensitivity of finite element analyses simulating punching failures to some model parameters like the constitutive law of concrete, the level of ductility available both after tensile cracking (tension softening) and after peak compression (compression softening), the effect of confinement and lateral cracking on compression law. Three experimental tests representing the three most common configurations for column-slab connection (central, edge and corner column) have been modelled with 15 analyses each. Quite good accuracy and small scattering of the results have been achieved on the prediction of ultimate punching load, whereas wider scattering has been observed on ultimate displacement.

The amount of available ductility in tensile and compressive behaviour related to the crack bandwidth value is a key parameter, as already observed by the same authors on other types of reinforced concrete failures such as deep beams and concrete walls [21], [22], [23], [24]. The results confirm the possibility to predict with accuracy punching failure without shear reinforcement using nonlinear FEM models. The presented analyses indicate that the proposed model can be used in future parametric studies on different aspects influencing punching shear in concrete slabs.

References

[1] J.G.M. Wood, “Pipers Row Car Park, Wolverhampton Quantitative Study of the Causes of the Partial Collapse on 20th March 1997”, SS&D Contract Report to HSE http://www.hse.gov.uk/research/misc/pipersrowpt1.pdf, 2002

[2] H. Salem, H. Issaa, H. Gheith, A. Farahata, “Punching shear strength of reinforced concrete flat slabs subjected to fire on their tension sides”, HBRC Journal, Vol. 8, No. 1, pp. 36-46.

[3] S. King, and N. Delatte, "Collapse of 2000 Commonwealth Avenue: Punching Shear Case Study." J.Perform.Constr.Facil., 18(1), pp. 54-61, 2012

[4] W. Bu, and M. A. Polak, “Seismic retrofit of reinforced concrete slab-column connections using shear bolts”, ACI Struct J, 106 (4), pp. 514–22, 2009

[5] H. Ingvarsson, *Betongplattors hållfasthet och armeringsutformning vid hörnpelare* (Load-bearing capacity of concrete slabs and arrangement of reinforcement at corner columns). Department of Structural Engineering, The Royal Institute of Technology, Meddelande Nr 122, Stockholm, Sweden, 1977, 143 pp., 1977

[6] S. Kinnunen, "*Försök med betongplattor understödda av pelare vid fri kant (Test on concrete slabs supported on columns at free edges)"*. Statens institut för byggnadsforskning, Rapport R2, Stockholm, 1971, 103 pp., 1971
[7] S. Kinnunen, H. Nylander, "Punching of Concrete Slabs Without Shear Reinforcement". Transactions of The Royal Institute of Technology, No.158, Stockholm, Sweden, 1960, 112 pp., 1960
[8] C. E. Broms, "Punching of flat plates – a question of concrete properties in biaxial compression and size effect". *ACI Structural Journal*, Vol. 87, No. 3, May-June 1990, pp. 292-300, 1990
[9] A. Muttoni and M. Fernández-Ruiz, "Shear strength of members without transverse reinforcement as function of critical shear crack width". *ACI Struct J*, 105, 163–172, 2008
[10] A. Cladera, A. Marí, J. M. Bairán, C. Ribas, E. Oller and N. Duarte, "The compression chord capacity model for the shear design and assessment of reinforced and prestressed concrete beams". *Structural Concrete*, vol. 17: pp. 1017–1032, doi:10.1002/suco.201500214, 2016
[11] L. Cavaleri, F. Di Trapani, M. F. Ferrotto, L. Davì, "Stress-strain models for normal and high strength confined concrete. Test and comparison of literature models reliability in reproducing experimental results". *Ingegneria Sismica*, vol. 34, pp. 114-137, 2017
[12] E. Thorenfeldt, A. Tomaszewicz, and J. J. Jensen, "Mechanical properties of high-strength concrete and applications in design", *In Proc. Symp. Utilization of High-Strength Concrete* (Stavanger, Norway) (Trondheim), Tapir. 1987
[13] F. J. Vecchio, and M. P. Collins, "Compression response of cracked reinforced concrete", *J. Str. Eng.*, ASCE 119, vol. 12, pp. 3590–3610, 1993
[14] P. H. Feenstra, "Computational Aspects of Biaxial Stress in Plain and Reinforced Concrete", PhD thesis, Delft University of Technology, 1993.
[15] European Committee for Standardization, Eurocode 2: Design of Concrete Structures: Part 1: General Rules and Rules for Buildings. 2002.
[16] D. A. Hordijk, "Local Approach to Fatigue of Concrete". PhD thesis, Delft University of Technology, 1991
[17] J. Oliver, M. Cervera, S. Oller, "Isotropic damage models and smeared crack analysis of concrete", *Proceedings of SCI-C* 1990, pp. 945–958. 1990
[18] CEN, Comité Européen de Normalisation, "EN 1992-1-1 - Eurocode 2 - Design of concrete structures – Part 1-1: General rules and rules for buildings", 2004.
[19] American Concrete Institute (ACI) Committee 318, Building Code Requirements for Structural Concrete (ACI 318-08) and Commentary, 2008
[20] Fédération Internationale du Béton (*fib*), "Fib model code for concrete structures 2010". Berlin, Germany: Wilhelm Ernst & Sohn, 2013
[21] G. Bertagnoli, G. Mancini, A. Recupero, N. Spinella, "Rotating compression field model for reinforced concrete beams under prevalent shear actions", *Structural Concrete*, vol.12, No.3 pp. 178-186, 2011
[22] G. Bertagnoli, D. La Mazza, G. Mancini, "Effect of concrete tensile strength in non linear analyses of 2D structures - a comparison between three commercial finite element softwares", *3rd International Conference on Advances in Civil, Structural and Construction Engineering - CSCE 2015*, Roma, 10-11 December, pp. 104-111, 2015
[23] G. Mancini, G. Bertagnoli, D. La Mazza, D. Gino, "Comparison between non-linear numerical models for R.C. shear walls under cyclic loading". *Italian Concrete Days Giornate AICAP 2016 Congresso CTE*, Roma, 27-28 October, pp. 1-8, 2016
[24] D. Gino, G. Bertagnoli, D. La Mazza, G. Mancini, "A Quantification of Model Uncertainties in NLFEA of R.C. Shear Walls subjected to Repeated Loading", *Ingegneria Sismica*, vol. 34, Special issue, pp. 79-91, 2017